

Strong Gate Coupling of High- Q Nanomechanical Resonators

Jaakko Sulkkö,[†] Mika A. Sillanpää,^{*,†} Pasi Häkkinen,[†] Lorenz Lechner,[†] Meri Helle,[†] Andrew Fefferman,[‡] Jeevak Parpia,[§] and Pertti J. Hakonen[†]

[†]Low Temperature Laboratory, Aalto University, P.O. Box 15100, FI-00076 Aalto, Finland, [‡]University of California, Berkeley, Berkeley, California 94720, United States, and [§]Department of Physics and LASSP, 608 Clark Hall, Cornell University, Ithaca New York 14853-2501, United States

ABSTRACT The detection of mechanical vibrations near the quantum limit is a formidable challenge since the displacement becomes vanishingly small when the number of phonon quanta tends toward zero. An interesting setup for on-chip nanomechanical resonators is that of coupling them to electrical microwave cavities for detection and manipulation. Here we show how to achieve a large cavity coupling energy of up to (2π) 1 MHz/nm for metallic beam resonators at tens of megahertz. We used focused ion beam (FIB) cutting to produce uniform slits down to 10 nm, separating patterned resonators from their gate electrodes, in suspended aluminum films. We measured the thermomechanical vibrations down to a temperature of 25 mK, and we obtained a low number of about 20 phonons at the equilibrium bath temperature. The mechanical properties of Al were excellent after FIB cutting, and we recorded a quality factor of $Q \sim 3 \times 10^5$ for a 67 MHz resonator at a temperature of 25 mK. Between 0.2 and 2 K we find that the dissipation is linearly proportional to the temperature.

KEYWORDS Nanomechanics, NEMS, quantum limit, detection, dissipation

The measurement of small-amplitude vibrations in mechanical systems is becoming an increasingly interesting problem.^{1,2} From the point of view of basic science, the study of mechanical systems close to the quantum limit has attracted a lot of interest recently.^{3,4} The endeavor toward the ground state of the harmonic phonon oscillations has been going on in various physical systems such as in optomechanics^{5–7} or in electrically coupled beam resonators, which have been measured using single-electron transistors,^{4,8} or, lately, with on-chip microwave cavities.^{9–12}

The quantum challenge is posed by several issues, including the relatively low frequency ($f_0 \sim 10$ MHz), of the lowest modes in suspended beams. The quantum limit implies stringent requirements on temperature, since hf_0 needs to be small in comparison to $k_B T$. On the other hand, at higher frequencies, the coupling to measuring systems diminishes rapidly. Third, the zero-point vibration amplitudes

$$x_{\text{ZP}} = \sqrt{\hbar/2m\omega_0}$$

where m is the effective mass and $\omega_0 = 2\pi f_0$ is the angular frequency, are vanishingly small even at the atomic scale. Very recently, O'Connell et al.¹³ demonstrated a piezoelectric mechanical mode at the quantum ground state by using a coupling to a superconducting qubit. However, bringing a purely mechanical mode to the quantum limit remains an ongoing quest, with the goal becoming a reality probably in the near future.

Micromechanical resonators are also used in applications as detectors. The best devices take advantage of the trend to smaller size and higher frequencies and will soon approach sensing at the atomic mass unit level.^{14,15} They could also be operated as sensors of position, force, or high-frequency electromagnetic fields.

For conductive resonators, capacitive coupling to an electrical measuring apparatus is useful for readout. In contrast to magnetomotive or optical detection, one can obtain very low electrical losses. An impediment to capacitive measurement is the reduction of coupling with increasing frequency that accompanies reduction in size. The coupling via a capacitance C_g is proportional to dC_g/dx , which for typical geometries depends on the vacuum gap x_0 between the vibrating beam and the gate electrode as $(x_0)^{-2}$, and hence small gaps are crucial. Using traditional e-beam fabrication, it is hard to obtain x_0 below 100 nm. Here we show that focused ion beam (FIB) milling yields gaps down to ~ 10 nm for resonator beams up to 10 μm in length and 100–200 nm in thickness. An improvement in coupling by 2 orders of magnitude can thus be achieved using FIB techniques. We also find that mechanical dissipation is reduced by the FIB milling, and we observe quality factors approaching half a million at dilution refrigerator temperatures.

Our system, as shown in Figure 2, is a flexural beam coupled capacitively to an LC cavity resonator detuned substantially from the beam's frequency, i.e., $f_{\text{LC}} \gg f_0$. The beam displacement x pulls the cavity frequency by the amount gx , where the coupling energy is

* Corresponding author. E-mail: Mika.Sillanpaa@iki.fi.

Received for review: 08/5/2010

Published on Web: 11/05/2010



$$g = (\omega_{LC}/2C)(\partial C_g/\partial x)$$

and

$$\omega_{LC} = 2\pi f_{LC}$$

In the quantum language, the Hamiltonian of the whole system is

$$\hat{H} = \hbar\omega_{LC}\hat{a}^\dagger\hat{a} + \hbar\omega_0\hat{b}^\dagger\hat{b} + \hbar g\hat{x}\hat{a}^\dagger\hat{a} - ig_V(\hat{b} + \hat{b}^\dagger)(\hat{a} - \hat{a}^\dagger)$$

Here, \hat{a}^\dagger and \hat{a} are the creation and annihilation operators of the cavity, and similarly \hat{b}^\dagger and \hat{b} are operators for the nanoresonator. $\hat{x} = x_{ZP}(\hat{b}^\dagger + \hat{b})$ is the quantum amplitude of the nanoresonator. The photon-exchange linear coupling with the energy

$$g_V = x_{ZP}V_g\sqrt{\frac{\hbar\omega_{LC}}{2C}}(\partial C_g/\partial x)$$

can be tuned up to a very high value with a dc voltage V_{dc} but is negligible unless the cavity and the nanoresonator are close to resonance.

We have used¹¹ shorter beams, $l \sim 1.5$ to $10 \mu\text{m}$, than in refs 10 and 12 and we obtain higher frequencies.¹⁶ Therefore, one would obtain low mechanical occupancies already at dilution refrigerator temperatures. The trade-off, however, is the smaller area for detection due to the shorter beam length when measuring via an LC cavity, as well as a reduction of gain as $\propto f_{LC}/f_0$. To this end, FIB processing offers a well suited method to make extremely narrow vacuum gaps for relatively short beams.

In our fabrication, we used focused ion beam (FIB) milling to separate the gate and the beam from a prefabricated, T-shaped, suspended structure, Figure 1. The prefabrication followed closely the steps presented in ref 11. A brief anneal

TABLE 1. Length, l , Width, t_x , Height, t_y , and the Vacuum Gap, x_0 , of the Measured Nanomechanical Resonators^a

sample	l (μm)	t_x (nm)	t_y (nm)	x_0 (nm)	f_0^{th} (MHz)	f_0^{exp} (MHz)
A	4.2	125	141	24	65	67.3
B	3.0	147	141	29	114	101.3
C	5.4	161	143	18	46	50.8
D	5.3	187	143	21	52	52.9
E	9.3	309	155	20	27	27.2
F	9.3	290	155	14	27	26.7

^a The resonance frequencies f_0 were measured at 4.2 K in a vacuum better than $\sim 10^{-4}$ mbar. The estimated frequency is given by $f_0 = (t_x/l^2)(E/\rho)^{1/2}[1 + \epsilon t_x t_y^2/(4\pi^2 I)]^{1/2}$, where E , $I = t_y t_x^3/12$, and ρ are, the Young's modulus, the second moment of inertia, and the density, respectively. $\epsilon = \Delta l/l \sim 0.6\%$ denotes the tensile strain. f_0^{th} and f_0^{exp} denote the calculated and measured mechanical resonance frequencies, respectively.

at 250 °C for 30 min was performed to generate a built-in tensile strain before cutting. In order to avoid contamination, the FIB modification was performed without exposing nearby structures to the Ga beam. This was achieved by dual beam operation with careful across-beam alignment (dual beam microscope, Helios Nanolab, FEI, Ltd.). The line cut was performed at 30 keV in single-pass mode, instead of gradually scraping the surface, in order to exploit differential sputtering effects which allow smaller gap dimensions and significantly reduce Al redeposition onto the structure. Vacuum gaps of 50–10 nm were obtained by an appropriate choice of the ion beam diameter (minimum diameter ~ 5 nm). The dimensions of the measured samples are listed in Table 1.

An interesting issue in the fabrication process is that of possible side-effects of FIB milling on the sidewalls of the slit. These include Ga implantation, amorphization, heating,

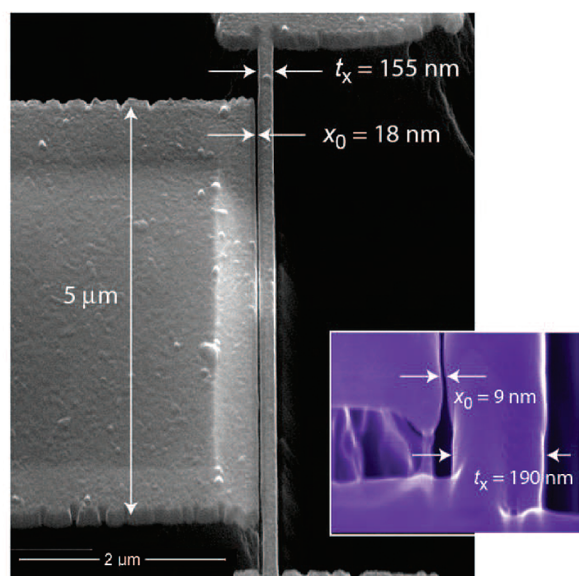
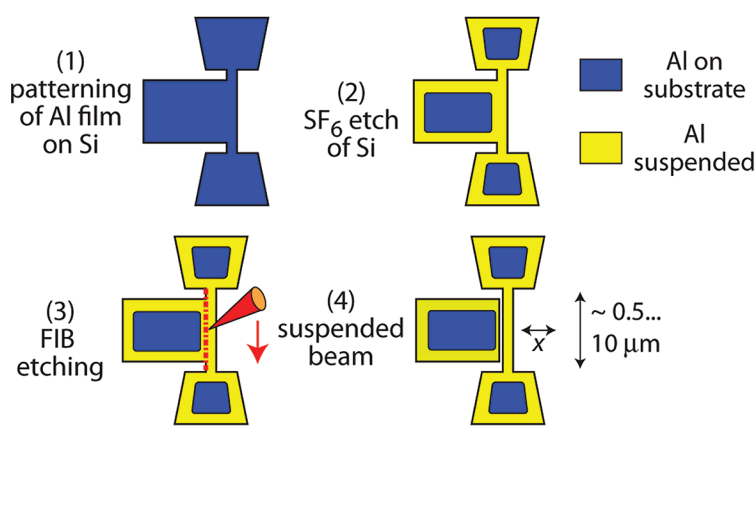


FIGURE 1. The fabrication of strongly capacitive coupled nanoresonators, (1–4), on top of a high-resistivity silicon wafer. E-beam lithography was used to pattern the metallization. Before focused ion beam (FIB) milling, the e-beam evaporated aluminum T-structure was suspended by an optimized SF_6 reactive ion etch. The single-pass line cut, with current 10 pA, milling depth ~ 100 nm, and diameter ~ 5 nm at 30 kV, gives vacuum gaps down to 10 nm without any noticeable bending of the beam. On the right, SEM image of a beam-gate structure (sample C). The detail shows a short beam with $a < 10$ nm gap and typical rounded cross section seen after milling.

and generation of defects. Investigations of these artifacts have mainly concentrated on substrate materials and semiconductors.^{17,18} However, some general conclusions can be made on the basis of our process parameters. The thickness of the sidewall layer with damage is on the order of 10–30 nm for the employed beam energy of 30 kV.^{17–19} Since this is not negligible in comparison to the width of our beams, both mechanical as well as electrical properties may be altered by the FIB-induced damage.

The damage is known to lead to stress enhancement in the milled structures, due to either formation of solid solution or Taylor or precipitation hardening.^{19–21} Ion doses required to cut the film led to bent beams, an indication of compressive strain induced in the surface exposed to milling. Stress effects were negligible for beams of relatively low aspect ratio $l/t_x \lesssim 30$, confirmed by the uniform structure in Figure 1. We use differential thermal contraction to estimate the additional stress on cooling, $T_0 \sim Et_x t_y (\Delta l)/l$ with $\Delta l/l \approx 4 \times 10^{-3}$. Together with $E = 70$ GPa and an initial stress of 0.15 GPa, we obtain resonant frequencies within 10% of those listed in Table 1.

We first detected and characterized the flexural vibrations by electric actuation through the gate capacitance, see ref 11 as in Figure 2. In order to maximize the coupling, the stray capacitance C in parallel to the beam should be minimized. For the best setup (sample E), we used an on-chip spiral coil inductor with 15 turns and 3 μm line width. The stray capacitance was further reduced by removal of a substantial part of the underlying substrate by the Si etch. The values $C \approx 30$ fF, $L = 14.5$ nH were obtained from

electromagnetic simulation of the structure, and which agree with the measured $f_{LC} = 7.64$ GHz. For the other samples (apart from E), we used off-chip inductors with $C \sim 0.3$ pF, and $L \sim 3\text{--}10$ nH. The cavity line width is adjusted by the tuning capacitor $C_T \sim 1\text{--}5$ pF such that $\Delta f_{LC} \lesssim f_0$.

The force driving the beam is given as

$$F(t) = \frac{1}{2} V_g^2(t) \frac{dC_g}{dx}$$

The mechanical motion gives rise to a time-varying capacitance

$$C_g(t) = C_{g0} + \left(\frac{\partial C_g}{\partial x} \right) x$$

The variation of the total capacitance of the LC resonator leads to its frequency modulation, which creates sidebands at $f_{\pm} \equiv f_{LC} \pm f_0$ in a microwave reflection measurement. The blue sideband voltage V_+ was directly measured by a spectrum analyzer as shown in Figure 2a. As a first amplification stage, we employed preamplifiers with a noise temperature T_N varying between ~ 3 and 300 K. Two circulators in cascade were employed to reduce preamplifier backaction noise. The low-temperature measurements were performed in a dilution refrigerator that also provides an ultrahigh vacuum environment.

Figure 2b displays the driven response for a 5 μm long Al beam with a gap of 21 nm (sample D in Table 1). The peaks were measured by sweeping f_g and stepping V_1 by 10 dB between successive spectra. We observe a linearly increasing Lorentzian response, which displays a Duffing-type instability (stiffening spring) at deflections on the order of 2 nm as expected for a doubly clamped beam resonator.

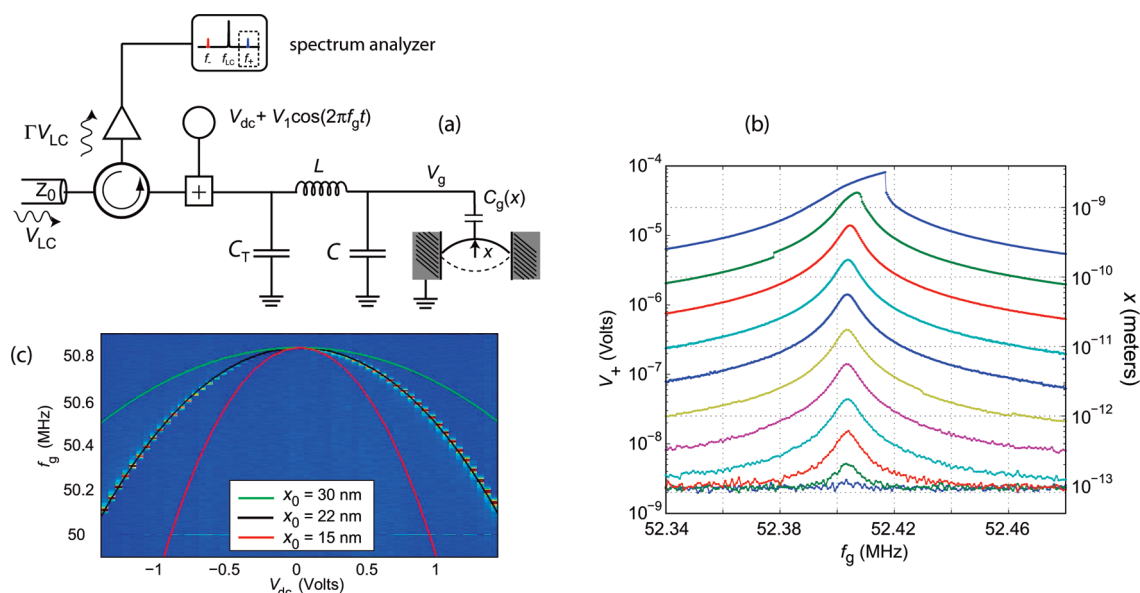


FIGURE 2. (a) Reflection measurement scheme for the detection of nanomechanical vibrations coupled capacitively to the electrical resonance frequency of a cavity (lumped element LC circuit in the figure), $f_{LC} = f_{LC}(1 + gx)$. The vibrations of the beam at the mechanical frequency $f_0 \ll f_{LC} \approx (LC)^{-1/2}/2\pi$ change the total capacitance. The resulting sideband voltage is measured by a spectrum analyzer. The inductive coupling of the cavity allows for introducing a dc voltage to the gate. (b) Electrically actuated response of a 5.4 μm long nanomechanical resonator (sample D) as a function of mechanical drive frequency f_g measured at $T = 4.2$ K, with voltages $V_{dc} = 0.2$ V and $V_{LC} \approx 1$ mV, while the drive for the mechanical mode V_1 is increased from bottom (60 nV) to top (6 mV) at 10 dB intervals. (c) Resonance measured as a function of dc bias V_{dc} (sample C). The solid curves display the calculated dependence at gap values x_0 indicated in the figure.

In Figure 2c we display the measured sideband resonance position as a function of dc bias V_{dc} . The concave parabolic shape with gate voltage is characteristic of resonators with small tension. Since the dc voltage dependence becomes very sensitive to the vacuum gap x_0 at small separations, this dependence can be used for verification of the gap size. Indeed, we obtain the best fit for a gap which is close to that seen in an SEM image (18 nm), whereas larger values are clearly excluded. The solid curves display the calculated dependence modeling the capacitance

$$C_g = \pi\epsilon_0 l \left\{ \ln[x_0/t_y + 1 + \sqrt{(x_0/t_y)^2 + 2x_0/t_y}] \right\}^{-1}$$

This estimate gives, for instance, $C_g \sim 0.5$ fF for sample E. We also infer that the FIB processed regions remain metallic.

Attempts to cool mechanical systems down to the quantum ground state have usually taken place at relatively low frequencies, using active feedback cooling, or by passive sideband cooling.^{5,10,12} With the latter method, occupation quanta number ~ 4 was recently obtained.¹² At higher frequencies, electrical cooling is not necessary to achieve low quantum occupation, as demonstrated by the Cleland group.¹³ For our resonators around 50 MHz, relatively low occupancies are feasible already without sideband cooling.

We measured the thermomechanical vibrations at several different temperatures for the 9 μm long beam, sample E. The temperature was simultaneously monitored by a primary Coulomb blockade thermometer. The noise floor is set by the cold amplifier noise, $T_N \sim 2.5$ K.

We fitted a Lorentzian (representing the thermal vibration peak), plus the noise floor to the measured sideband power; see insets of Figure 1. The area A under the peak, given by the parameters of the fitted Lorentzian, is directly proportional to the energy of the vibration degree of freedom but requires knowledge of the system gain which is difficult to deduce accurately. At higher temperatures, we assume that the beam is thermalized and calibrate the area of the peak against $k_B T = A = n\hbar\omega_0$. We obtained linear behavior, see Figure 1, of A against T down to the base temperature of 26 mK, and hence infer a low number of quanta ~ 20 at 26 mK.

The coupling energy g between the resonator and cavity can be estimated using the parameters of the cavity, and $dC_g/dx \approx 10$ nF/m based on the dimensions of the beam and the gap. The model is verified by the dc voltage dependence; see Figure 2. We obtain an order of magnitude larger coupling $g \sim 2\pi \times 1$ MHz/nm than previously demonstrated.^{10,12,22}

A high mechanical quality factor Q_m is instrumental for various detector applications, as well as sideband cooling near the quantum ground state, and to observe phenomena in that regime. The losses are often dominated by defects which influence the mechanical and thermodynamic properties of amorphous materials at low temperatures,²³ described using two level tunneling states (TLS). Typically, the quality factor decreases with the physical size of the resona-

tor, an indication that surface losses pose a bottleneck.² A suitable figure of merit to take into account both frequency and Q value is their product, $f_0 Q_m$. For sample A, we obtain, with the lowest mode at 67 MHz and $Q_m = 2.7 \times 10^5$ at $T = 25$ mK, $f_0 Q_m \approx 2 \times 10^{13}$ Hz.

Interestingly, we observed that the Q value seemed to be improved by the FIB milling. A test sample fabricated using a single e-beam lithography step, having $l = 2.5 \mu\text{m}$, $f_0 = 105$ MHz, displayed an order of magnitude lower $Q_m = 25 \times 10^3$ at $T = 25$ mK. The improvement of Q can be due to modification of the properties of microscopic defects. A more complicated scenario could be envisioned owing to the compressive strain generated by the FIB cutting at the edges of the beam. This would cause the edges to have less strain than the rest of the beam. Therefore the stress due to flexural motion, which is usually concentrated near the beam edge would be more uniformly distributed over the beam. The coupling of phonons to defects depends on the strength of the local strain field and, thus, is reduced.

We also investigated the temperature dependence of the performance of some of the samples. We used the driven response, as in Figure 2b, or a different approach which uses two microwave frequencies f_{LC} and f_2 such that $f_2 - f_{LC} \sim f_0$.²⁶ Both methods gave similar results. In the latter case, the low-frequency force driving the mechanics is now $\propto V_{LC} V_2$, where V_{LC} and V_2 are the microwave voltages. f_2 was kept constant, while reflection at f_{LC} was swept with a vector network analyzer. We find a strong decrease in the dissipation Q_m^{-1} with decreasing temperature in the range 0.1–2 K; see Figure 4. Our data follow approximately $Q_m^{-1} \propto T$ in this range. This behavior is qualitatively similar to that observed in latest experiments measured in a considerable magnetic field. Much weaker T dependence was obtained in amorphous gold resonators.²⁴ Hoehne et al.²⁵ obtained recently a similar linear temperature dependence in lithographically patterned Al resonators. Therefore, we conclude that while the dissipation is decreased due to FIB processing, its source likely stays unchanged. Notice that the saturation below 0.1 K is not due to thermal decoupling, since we observe a consistent linear dependence of the thermal vibration energy down to 26 mK; see Figure 3.

The mechanical resonance frequency f_0 was also found to depend on T , although rather weakly: at $V_{dc} = 0.2$ V, $\delta f/f_0 \approx 2 \times 10^{-5} \ln(T/T_0)$ while at $V_{dc} = 0.8$ V, we find $\delta f/f_0 \approx 4 \times 10^{-5} \ln(T/T_0)$. Since $(\partial f_0)/(\partial V_{dc})$ grows with V_{dc} , part of the frequency shift can be attributed to changes in the dielectric constant of the substrate material.

The logarithmic temperature dependence of $\delta f/f_0$ and the rolloff in $1/Q_m$ observed here (Figure 4) are qualitatively consistent with those predicted by TLS and explained by the tunneling model.²³ In this model, the former is due to the resonant interaction between drive phonons and TLS. The rolloff in $1/Q_m$ is observed at the temperature $T_{CO} \sim 1$ K at which the relaxation rate of the TLS (τ^{-1}) equals the mechanical

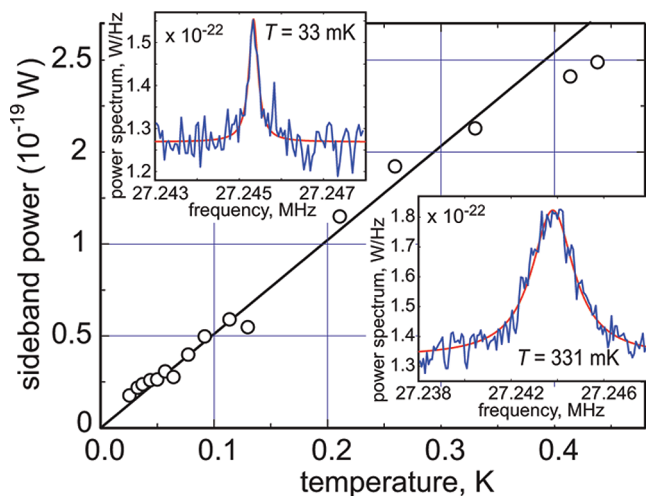


FIGURE 3. The total energy of the thermomechanical vibration peak measured for sample E ($f_0 = 27$ MHz) as a function of the cryostat temperature. Linear behavior is observed down to the base temperature of 26 mK, where we obtain a low number of quanta, $n \sim 20$, without electrical cooling via the cavity. The insets show the thermal vibration spectra measured at two different temperatures. The red lines are fits (see text). The width of the peaks changes due to the strong temperature dependence of the mechanical quality factor.

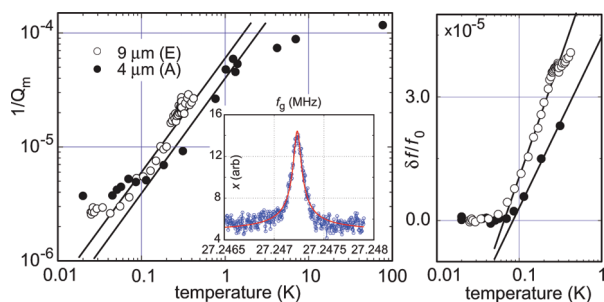


FIGURE 4. Measured temperature dependence of the inverse mechanical quality factor (samples A and E). The solid line indicates $\propto T$ dependence. The inset is an example of the driven response (sample E), at $T = 25$ mK, fitted to a Lorentzian which yields $Q_m \approx 3.64 \times 10^5$. The right frame shows the corresponding change in the mechanical frequency, together with a logarithmic fits.

frequency, $\omega_0\tau = 1$. This is consistent with that observed in ref 27, since T_{CO} varies as $\omega^{1/3}$.

The temperature dependence of $1/Q_m$ for $T < T_{CO}$ depends on the dominant relaxation mechanism (electron-driven or phonon-driven) and size effects. Electron-driven relaxation produces a linear temperature dependence of $1/Q_m$ for $T < T_{CO}$. However, here, in the superconducting state, one expects that phonon-driven relaxation should dominate.²⁸ Yet the T^3 dependence of $1/Q_m$ expected for $T \ll T_{CO}$ due to relaxation driven by 3D phonon modes²⁹ is not developed, perhaps because other dissipation mechanisms become important at the lowest temperatures.

The dominant thermal phonon wavelength in Al, ~ 37 nm K/T, becomes comparable to the widths and thicknesses of the beams at 100–300 mK.³¹ In this limit, the dominant

modes are no longer 3D phonon modes³² and can contribute a linear temperature dependence.^{25,30} This mechanism thus could dominate relaxational damping in our high-frequency resonators. At the lowest temperatures, the resonant contribution to $1/Q_m \propto \tanh(\hbar\omega/2k_B T)$ may contribute to the measured saturation.

The large capacitive coupling we have achieved between a nanoresonator and an LC circuit can be useful for various sensitive detectors. The responsivity of the signal voltage to a mass change is $dV/dm \sim VQ_m/m$. For our sample (E) setup at $T = 4$ K as in Figure 2, we obtain $s_m \sim 10^{-26}$ kg/Hz^{1/2} ~ 10 AMU/Hz^{1/2}, which would improve the state of the art¹⁴ of mass detection by an order of magnitude. For studies near the quantum limit, the strong coupling achieved via FIB milling is a critical asset since it enables Q -enhanced high-frequency resonators. Indeed, for short beams 1–2 μm in length, we have obtained vacuum gaps approaching 5 nm. These findings substantially improve, for example, the efficiency of electrical cooling via the LC circuit which is inversely proportional to the fourth power of the gap.

Acknowledgment. We thank T. Heikkilä and H. Seppä for fruitful discussions. This work was supported by the Academy of Finland, and jointly by the NSF under DMR-0908634 (Materials World Network) and the Academy of Finland, the ERC Contracts FP7-240387, EU FP6-IST-021285-2, and the NANOSYSTEMS project with Nokia Research Center.

REFERENCES AND NOTES

- (1) Cleland, A. *Foundations of Nanomechanics*; Springer: New York, 2003.
- (2) Ekinci, K. L.; Roukes, M. L. *Rev. Sci. Instrum.* **2005**, *76*, No. 061101.
- (3) Schwab, K. C.; Roukes, M. L. *Phys. Today* **2005**, *58*, 36–42.
- (4) LaHaye, M. D.; Buu, O.; Camarota, B.; Schwab, K. C. *Science* **2004**, *304*, 74–77.
- (5) Metzger, C.; Karrai, K. *Nature* **2004**, *432*, 1002–1005.
- (6) Gigan, S.; et al. *Nature* **2006**, *444*, 67–70.
- (7) Schliesser, A.; Del'Haye, P.; Nooshi, N.; Vahala, K. J.; Kippenberg, T. J. *Phys. Rev. Lett.* **2006**, *97*, 243905.
- (8) Knobel, R. G.; Cleland, A. N. *Nature* **2003**, *424*, 291–293.
- (9) Truitt, P. A.; Hertzberg, J. B.; Huang, C. C.; Ekinci, K. L.; Schwab, K. C. *Nano Lett.* **2007**, *7*, 120–126.
- (10) Regal, J. D.; Teufel, C. A.; Lehnert, K. W. *Nat. Phys.* **2008**, *4*, 555–560.
- (11) Sillanpää, M. A.; Sarkar, J.; Sulkko, J.; Muhonen, J.; Hakonen, P. J. *Appl. Phys. Lett.* **2009**, *95*, No. 011909–011911.
- (12) Rocheleau, T.; Nduduk, T.; Macklin, C.; Hertzberg, J. B.; Clerk, A. A.; Schwab, K. C. *Nature* **2009**, *463*, 72–75.
- (13) O'Connell, A. D.; et al. *Nature* **2010**, *464*, 697–703.
- (14) Jensen, K.; Kim, K.; Zettl, A. *Nat. Nanotechnol.* **2008**, *3*, 533–537.
- (15) Lassagne, B.; Garcia-Sanchez, D.; Aguasca, A.; Bachtold, A. *Nano Lett.* **2008**, *8*, 3735–3738.
- (16) Li, T. F.; Pashkin, Y. A.; Astafiev, O.; Nakamura, Y.; Tsai, J. S.; Im, H. *Appl. Phys. Lett.* **2008**, *92*, No. 043112–043114.
- (17) McCaffrey, J. P.; Phaneuf, M. W.; Madsen, L. D. *Ultramicroscopy* **2001**, *87*, 97–104.
- (18) Wang, Z.; Kato, T.; Hirayama, T.; Kato, N.; Sasaki, K.; Saka, H. *Appl. Surf. Sci.* **2005**, *241*, 80–86.
- (19) Kiener, D.; Motz, C.; Rester, M.; Jenko, M.; Dehm, G. *Mater. Sci. Eng., A* **2007**, *459*, 262–272.
- (20) Bei, H.; Shim, S.; Miller, M. K.; Pharr, G. M.; George, E. P. *Appl. Phys. Lett.* **2007**, *91*, 111915–111917.

- (21) Samayoa, M. J.; Haque, M. A.; Cohen, P. H. *J. Micromech. Microeng.* **2008**, *18*, 95005–95011.
- (22) Teufel, J. High coupling energies were also recently demonstrated in a different geometry. Personal communication, 2010.
- (23) Phillips, W. A. *Rep. Prog. Phys.* **1987**, *50*, 1657–1708.
- (24) Venkatesan, A.; Lulla, K. J.; Patton, M. J.; Armour, A. D.; Mellor, C. J.; Owers-Bradley, J. R. *Phys. Rev. B* **2010**, *81*, No. 073410.
- (25) Hoehne, F.; Pashkin, Yu. A.; Astafiev, O.; Faoro, L.; Ioffe, L. B.; Nakamura, Y.; Tsai, J. S. *Phys. Rev. B* **2010**, *81*, 184112.
- (26) Viikari, V.; Seppä, H. *IEEE Sens. J.* **2009**, *9*, 1918–1923.
- (27) Fefferman, A.; Pohl, R. O.; Parpia, J. M. Submitted to *Phys. Rev. B*, **2010**.
- (28) Black, J. L.; Fulde, P. *Phys. Rev. Lett.* **1979**, *43*, 453–456.
- (29) Fefferman, A. D.; Pohl, R. O.; Zehnder, A. T.; Parpia, J. M. *Phys. Rev. Lett.* **2008**, *100*, 195501.
- (30) Seoanez, C.; Guinea, F.; Castro Neto, A. H. *Phys. Rev. B* **2008**, *77*, 125107.
- (31) Klitsner, T.; Pohl, R. *Phys. Rev. B* **1987**, *36*, 6551–6565.
- (32) Landau, L. D.; Lifshitz, E. M. *Theory of Elasticity*; Pergamon: London, 1959.